

TOTAL LIGHTNING CHARACTERISTICS OF ORDINARY CONVECTION

Shane M. Motley¹, Lawrence D. Carey^{1*}, Brandon L. Ely¹, R. E. Orville¹, J. Guynes¹, and Martin J. Murphy²

¹Texas A&M University, College Station, Texas, USA

²Vaisala Corporation, Tucson, Arizona, USA

1. INTRODUCTION

With the advent of continuously operational three-dimensional (3-D) lightning mapping systems, complete observations of a thunderstorm's lightning development are now routinely available. Recent studies examining correlations between three dimensional (3-D) lightning flash characteristics and convective intensity (e.g., magnitude of updraft) and state (e.g., early, mature and dissipating phases) have shown promising results; however, emphasis has focused primarily on complex modes of convection (e.g., supercells and squall lines), often with only a limited portion of the cell's lifetime examined (e.g., Ray et al. 1987; Coleman et al. 2003; Lang et al. 2004a,b; Carey et al. 2005; Wiens et al. 2005; Steiger et al. 2005). Although it is the most ubiquitous and fundamental cell type, ordinary, single-cell convection has received relatively little recent attention in the lightning community. Placing emphasis on ordinary convection allows for a more direct approach to the complex evolution of the microphysical and kinematic processes involved in the electrical development of thunderstorms.

Devising methods to associate the evolution of lightning and inferred charge structure to convective intensity and state requires an accurate and detailed depiction of 3-D total lightning data. Utilizing instruments that locate lightning radiation at VHF frequencies (very high frequency) enables the in-cloud parts of both intracloud (IC) and cloud to ground (CG) flashes to be studied. In addition, inferences on storm charge structure are possible with the use of VHF source densities (Mazur et al. 1997; Rison et al. 1999; Thomas et al. 2001) because the negative end of a bidirectional leader produces large

amounts of VHF radiation (Shao and Krehbiel, 1996). Therefore, regions of high VHF source densities suggest areas of positive charge regions.

Past studies suggest that the gross charge structure of a thunderstorm resembles a dipole or tripole structure of charge with the main negative charge region located around the -10°C to -20°C isotherm (e.g., Williams 1989; MacGorman and Rust 1998). However, it is understood that more complex vertical charge structures can exist within convection, with up to 4 or 5 layers of charge (Stolzenburg et al. 1998). Some of these additional charge structures can be attributed to screening layers that develop as a result of discontinuities in conductivity at the boundary of clouds (MacGorman and Rust 1998). Typically, the layers of charge associated with screening layers are very thin and, unlike main charge regions, the locations of screening layers are difficult to assess with VHF lightning observations. Therefore, our emphasis will focus on the development of the gross charge structure of the conventional tripole model.

Mounting evidence suggests that the origin of the main negative charge region is the ice-ice collisional (or non-inductive) charging mechanism (e.g., Takahashi 1978). Rebounding collisions between graupel and ice crystals in the presence of supercooled water result in the particle scale separation of charge with negative (positive) charge on the graupel (ice crystal). Differential sedimentation and an increasing updraft speed with height result in the storm scale separation of charge and the classical thunderstorm dipole of positive over negative charge.

Most intracloud (IC) lightning flashes originate between the main negative and the upper positive charge regions (Shao and Krehbiel 1996). Several studies have documented this prevalence of IC lightning over CG lightning in the early stages of convective development. Williams et al. (1989) suggests this relationship is due to the accumulation of graupel particles in the center of the dipole region in the developing and mature

* *Corresponding author address:* Dr. Larry Carey, Dept. Atmospheric Sciences, Texas A&M University, College Station, Texas 77843-3150; larry_carey@tamu.edu

stages of thunderstorms and the subsequent descent of ice particles below the height of the negative charge region as downdrafts begin to dominate. This subsequent descent of ice particles leads to the development of a lower positive charge region via the non-inductive and/or inductive (MacGorman and Rust 1998) charging mechanisms. Past research suggests that the lower positive charge region provides the bias necessary for the onset of negative polarity CG flashes (e.g., Williams 1989). Supporting the Williams et al. (1989) results, Carey and Rutledge (1996) found a strong correlation between polarimetric radar inferred graupel volume and the IC flash rate. This study also found relations between the polarity of the electrical field and the amount and vertical location of ice within the storm. These ideas suggest that correlations may exist between the state of a thunderstorm (e.g. intensifying, weakening) and total lightning data. Examination of a statistically significant quantity of air mass thunderstorms allows further exploration of the conventional model for the development of gross charge layers and lightning development. In addition it is possible to examine whether significant correlations exist between lightning flash characteristics and radar inferred convective intensity and state.

Hypothesizing significant correlations between total flash characteristics and convective cell structure, intensity and state, we examined time-height cross-sections of mean radar reflectivity, flash origin heights, and VHF source density during the entire lifecycle of each convective cell. Total and CG lightning flash rate were also plotted in conjunction with the flash origin information in effort to gain further insight on the evolution of total lightning.

2. DATA AND METHODOLOGY

Time and location data of VHF radiation sources were obtained from two 3-D lightning mapping networks: 1) Vaisala's Dallas-Fort Worth Lightning Detection and Ranging (LDAR-II) network located in Dallas-Fort Worth Texas, and 2) the Texas A&M University LDAR-II (TAMU LDAR-II) located in Houston Texas. Each location employed level-II WSR-88D data from the National Climatic Data Center (NCDC) (with KHGX covering the TAMU LDAR-II network and KFWS covering the LDAR-II network); and CG flash location, time and polarity from the National Lightning Detection Network (NLDN: owned and operated by Vaisala) for several ordinary convective cells that occurred from May of 2001 to September of 2005. The data from both the NLDN

and LDAR-II combine to form a complete dataset of total lightning data. The two-dimensional NLDN data provide the latitude-longitude location and time, polarity, and stroke multiplicity of cloud-to-ground flashes. These data were obtained from Vaisala, Inc., Tucson, AZ, which has established a network consisting of 106 sensors across the U.S. (Orville and Huffines 1999). The median accuracy of ground flash locations is approximately 500 m and the expected flash detection efficiency is > 85-90%, for events with peak currents above 5kA (Cummins et al. 1998). For our analysis, the NLDN data were post-processed such that individually recorded strokes were grouped into flashes. In addition, we removed positive flashes characterized by peak currents less than 10kA since these flashes are likely associated with misidentified IC lightning (Cummins et al. 1998; Wacker and Orville 1999a,b).

The VHF radiation produced by both IC flashes and the IC component of CG flashes is monitored by the LDAR-II network. The Dallas LDAR-II network is comprised of 7 VHF sensors with 20-30 km baselines centered on the Dallas-Fort Worth International Airport (e.g., Carey et al. 2005). The TAMU LDAR-II network is comprised of 12 sensors with an average baseline of 25 kilometers centered slightly northeast of downtown Houston at 29.79°N and 95.31°W. Both these systems monitor VHF sources which are produced during the breakdown process, marking the initiation of bipolar streamers (McGorman and Rust 1998). According to Loeb (1966), when the streamer amasses enough electrons, it becomes self-propagating with both positive and negative streamers occurring simultaneously and initiating in regions where the electric field is the highest (Coleman et al. 2003). The LDAR-II can readily detect the negative end of the leader due to the large amounts of VHF radiation produced during its development (Shao and Krehbiel 1996). Continuously propagating positive leaders, on the other hand, do not emit much VHF radiation and are often missed by the LDAR system (Proctor et al. 1988). Positive and negative ends of the discharge tend to propagate through regions of extrema in the electric potential profile that approximately correspond to regions of concentrated charge of the opposite polarity (Shao and Krehbiel 1996; Coleman et al. 2003). Therefore, given that the negative polarity breakdown, which the LDAR can easily detect, typically occurs in positive charge regions, the LDAR network becomes a useful tool for inferring gross charge structure within thunderstorms.

Detecting VHF radiation sources through time of arrival systems like the LDAR-II network still comes with its limitations. These limitations must be taken into consideration before more subtle inferences of charge structure can be made. One of the most important limitations to consider is the relative detection efficiency of VHF sources. The Dallas LDAR-II network can accurately map out flashes in 3-D within approximately 100 km of the center of the network, where the expected flash detection efficiency is greater than 90% (Carey et al. 2005). Similar results have been shown from the TAMU LDAR-II network (Ely et al. 2006). Another relevant measure of performance is the source detection efficiency which was estimated to be approximately 4% of its maximum value at 100 km for the Dallas LDAR-II network (Carey et al. 2005). Therefore, convective cells that did not remain within 100 km (75 km) from the center of the Dallas (TAMU) LDAR-II network throughout their lifetime were not included in this study. This limitation in the LDAR-II network was taken into careful consideration when making inferences of charge structure and total flash characteristics. Another limitation of the LDAR-II comes from the fact that the network is not particularly good at mapping radiation sources associated with stepped and dart leaders propagating toward the ground (Mazur et al. 1997). In addition, while the breakdown and ionization processes emit strongly in VHF, CG return strokes, which occur in previously ionized channels, emit in the Low Frequency (LF) to Very Low Frequency (VLF) range. Thus, time of arrival systems like the LDAR-II are primarily limited to registering the VHF radiation associated with the IC component of total lightning.

Grouping VHF source data into individual flashes was accomplished with the use of a NASA based flash algorithm, which was recently translated to Interactive Data Language (IDL). This IDL program uses spatial and temporal restrictions to group the LDAR-II VHF sources into flashes. The program determines if a source was a part of a flash based on the following criteria: the maximum duration of the flash cannot exceed 3 seconds, the maximum time lag between points in a flash cannot exceed 0.5 seconds, the maximum time delay between points in a branch cannot exceed 0.03 seconds, and points must be within 5 km of each other to be considered part of the same flash.

The location, convective state (e.g. developing, mature, dissipating), kinematic and microphysical properties of each convective cell

were inferred from the Dallas-Fort Worth (KFWS) and Houston (KHGX) WSR-88D data. Analysis of the radar data was performed using WDSS-II (Warning Decision Support System-Integrated Information) software (Hondl 2003) provided by the National Severe Storms Laboratory (NSSL). This software contains several algorithms that allow for quantitative analysis of the intensity of individual convective cells (e.g. Severe Hail Index (SHI) algorithm (Witt et al. 1998), Vertically Integrated Liquid (VIL)). A measure of the vertical integral of ice water content (M_{ice}) was performed in addition to the parameters output by WDSS-II where M_{ice} :

$$M_{ice} = 1000\pi\rho_i N_o^{3/7} \left(\frac{5.28 \times 10^{-18} Z_e^{ice}}{720} \right)^{4/7}$$

Where Z_e is the equivalent radar reflectivity factor, and N_o is the intercept parameter for an assumed inverse exponential distribution for ice. The Vertically Integrated Ice (VIL) allows us to quantify the amount of ice available for non-inductive charging. Identification and tracking of each convective cell was performed with the WDSS-II Storm Cell Identification and Tracking (SCIT) algorithm (Johnson et al. 1998). In an effort to obtain cells that were representative of air mass thunderstorms as described by Byers and Braham (1949), we employed certain criteria that were used to assess whether a cell could be a part of our sample. These criteria included:

- 1) Radar must capture the entire life span of the cell.
- 2) Distance from cell to center of the Dallas (TAMU) LDAR-II network could not exceed 100 km (75 km) during cell's life span.
- 3) Cell must remain isolated from other convective cells such that VHF sources from one cell could not enter another (tests were made for each cell in order to ensure this did not occur).
- 4) Cell did not undergo a merge or split during its lifetime.
- 5) Cell must be identified by WDSS-II algorithms for 30 minutes or greater.
- 6) 40 dBZ contour observed at or above -10° C level for at least one scan.
- 7) Cell has no appreciable tilt.

Since most convectively active days had several cells occurring at the same time, the LDAR-II data for a given day usually contained VHF source point information for a number of cells. Thus, if a cell met the required criteria it was necessary to separate the VHF sources associated

with the cell of interest from the plethora of VHF sources that occurred from all cells within range of the LDAR-II network. This was performed by constructing a cylinder around each cell such that VHF sources that fell outside the bounds of the cylinder would not be associated with the cell of interest (Fig. 1a). The center and radius of each cylinder were constructed based on the ice-ice collisional (or non-inductive) charging mechanism (Takahashi, 1978). The presence of a sufficient quantity of graupel or hail, with ice crystals and supercooled water for charging, is typically associated with radar echoes approaching 30-40 dBZ between the -10° C and -20° C isotherm level (Dye et al. 1986). Previous studies have also shown that the main negative charge region typically resides around the level of the -10° C isotherm (Krehbiel 1986). Using archived Fort Worth (Lake Charles and Corpus Christi) rawinsonde data from the NCDC, the height of the -10° C isotherm was determined for each Dallas (TAMU) case day. A weighted average based on the spatial distance between the Corpus Christi and Lake Charles soundings was used to determine the temperature profile over Houston. WDSS-II was then used to examine the reflectivity values of each cell at the height of the -10° C isotherm.

The center and radius of each cylinder were based on reflectivity values at the height of the -10° C isotherm with the center of the cylinder being placed at the maximum reflectivity value for each cell at that height. The radius of each cylinder extended out to the furthest 20 dBZ contour from the cell's center in effort to capture the most electrically active portion of each cell. Fig. 1a shows one of the more difficult cases in creating the bounds of each cell due to close proximity of another developing convective cell. The bounds in this case were drawn such that the locations of the flash origins, which typically reside in close proximity to the main negative charge region (Proctor 1991) for the cell of interest were separated by a considerable distance (in this case ~ 8 km) from other cells. Latitude and longitude information for the center of each cylinder was recorded using output from WDSS-II. This information was then combined with the flash output from the NASA flash algorithm such that only those flashes that had origins within the bounds of the cell were associated with the cell. Comparisons could then be made between radar reflectivity values and total lightning data (i.e. LDAR-II source points and CG data) by converting radar data from a polar to a Cartesian grid space using REORDER software (Oye and

Case 1995) and overlaying both data sets. Horizontal and vertical grid spacing for the reflectivity data were typically set at 2.0 km and 1.0 km, respectively. The relatively large grid spacing was necessitated by the routine use of the Volume Coverage Pattern-21 (VCP-21) by the KFWS and KHXG WSR-88D. VCP-21, or precipitation mode, was the most common scanning strategy used, which ultimately resulted in a few data gaps in the vertical reflectivity data. Despite these occasional gaps in the radar data, the smoothing creates a general idea of the vertical distribution of reflectivity values such that the two datasets (total lightning activity and radar reflectivity) can be overlaid. Several IDL programs were employed to compare various radar parameters against the cell total and vertical profile of flash density, flash origin density, and flash source density for several air mass thunderstorm cases. All data sets were placed on the same temporal scale such that accurate comparisons between data sets could be made. VHF source densities were normalized over a 5 minute period while CG and IC flash rates were smoothed using a 5-minute running average. The VHF source density was gridded at 1 km resolution in the vertical for time-height cross-sections. The flash algorithm was used to obtain the exact time and height of each flash origin, which was then overlaid on the radar reflectivity and VHF source density plots.

3. RESULTS

Twenty six ordinary convective cells, which met the aforementioned criteria, were selected for this study. Seventeen of these cells occurred over the TAMU LDAR-II network, while the other 9 cases occurred over the Dallas LDAR-II network. Table 1 shows the synoptic environment for each case day, which shows a low shear and moderately unstable environment as the typical synoptic setup for ordinary convective cells.

A representative case, hereafter referred to as cell 1, occurred on 5 August 2005 over the Dallas-Fort Worth LDAR-II network. Upper air data for 5 August 2005 were obtained from the 6 August 2005 00 UTC Dallas-Fort Worth (FWD) rawinsonde. Conditions on this day were marginally favorable for the development of air mass thunderstorms with 327 J kg^{-1} of Convective Available Potential Energy (CAPE), and a weakly sheared vertical wind profile. The height of the -10° C and -20° C isotherms were 6.0 km and 7.7 km above ground level, respectively.

As shown in Fig. 2a, the first VHF sources that were observed by the LDAR-II occurred

Table 1. Synoptic environment for each case day where CAPE is Convective Available Potential Energy; CIN is Convective Inhibition; 0-6 km Shear is the variation in the wind vector from the surface to a height of 6 km; -10° C Iso Height is the height, in kilometers, of the -10° C isotherm. Values show that a low shear, moderately unstable environment was typical for ordinary convective cells.

	CAPE (J kg ⁻¹)	CIN (J kg ⁻¹)	0-6 km Shear (ms ⁻¹)	-10° C Iso Height (km)
27-Jun-01	1678	118	8.2	5.9
22-Jul-01	503	172	11.3	6.4
5-Aug-05	163	206	1.5	6.4
6-Aug-05	1267	138	5.7	6.4
2-Aug-05	1441	96	4.1	6.3
8-Aug-05	1889	63	5.1	6.5
20-Aug-05	1150	108	3.6	6.8
25-Aug-05	2098	61	2.1	6.8
13-Sep-05	1305	22	7.7	6.7

approximately 22 minutes after the first radar echoes associated with the storm appeared (initiation; $t = 0$). This time coincided with radar reflectivity inferred rapid intensification, which occurred 24 minutes ($t = 24$ minutes) after initiation and was marked by the 30 dBZ core rising well above the -10° C isotherm (Fig. 2a). Several other radar parameters suggest a rapid intensification occurred around this time with VIL increasing from 5 to 13 kg m⁻², VII increasing from 67 to 159 kg * 10⁶, and a severe hail index (SHI) of 3 J m⁻¹ s⁻¹ (Fig. 3a). The total flash rates at this time remained in the 1 to 2 flash per minute range and appeared to be predominately IC flashes (Fig. 2b). The one exception was a CG flash that occurred at $t = 24$ minutes. This flash occurred only two minutes and twenty-seven seconds after the first VHF source was registered by the LDAR-II. A noticeable increase in total flash rate occurred just after the period of rapid intensification ($t = 36$) with total flash rates increasing to levels as high as 10 flashes per minute (Fig 2b). A dramatic increase in the mean height of flash origins also occurred after the rapid intensification with mean heights rising from 8879 m to a mean height of 12223 m with standard deviations of 993 m and 1851 m, respectively. The 95th percentile of flash origin heights shows also shows a significant increase from 7.7 km to 13.3 km just after the main peak in total flash rate.

Similar to the results found by Carey and Rutledge (1996), observations of the SHI and VII values in Fig. 2c suggests this rapid increase in flash origin heights and VHF source density is due

to an increase in the ice available for non-inductive charging. The increase in height of both the VHF sources and flash origin heights is most likely attributed to a rapid increase in updraft strength as inferred by the higher VIL values (Fig. 2c) and the increase in height of the 30 dBZ reflectivity contour during this time (Fig. 2a). This suggests that the increase in updraft is responsible for lofting the positive charge region to a higher elevation as found earlier by Krehbiel (1986). The bimodal distribution of VHF sources, which has been well documented in past studies (Krehbiel, 1986; Marshal and Rust, 1991; Shao and Krehbiel, 1996), was not evident until just after the intensification period. Many of the lightning flash origins closely followed the 30 dBZ contour and yet extended out to the 10 dBZ contour similar to the findings discussed by Proctor (1991).

The first sign of a low level extent of flashes occurs just after the peak convective intensity inferred from radar and marks the onset of several CG lightning flashes. As the cell starts to weaken slightly, a rapid decrease in the total flash rate occurs, while the CG flash rate increases slightly to a rate of 3 flashes per minute. A very noticeable bimodal distribution of flash origins develops with the top mode of flash origins closely following the 15 dBZ contour as the cell continues to weaken. During the dissipation phase, the total and CG lightning flash rates drop off to ≤ 1 flash per minute. Although the total flash rate and flash origin heights decrease to levels seen at the initial onset of lightning, which was a period of limited CG flash activity, many of the lightning flashes during the dissipating phase of the cell are actually CG flashes. All of these results closely follow the idea

of the descent of ice particles contributing to a lower positive charge region leading to the onset of CG lightning flashes (e.g., Williams 1989; Williams et al. 1989; Carey and Rutledge 1996).

Examination of all twenty six cases shows the average time from the first LDAR detected flash to the first NLDN detected CG was 5 minutes. The average time span between the first radar echoes associated with the cell to the first VHF source was approximately 19 minutes. In every case, the onset of the first VHF sources were marked by a rapid increase in the intensity of the cell as inferred from radar reflectivity. Twenty five out of the twenty six cases did not see the first VHF source until the 30 dBZ contour of radar reflectivity had risen above the -10°C isotherm. Several other radar parameters suggest rapid intensification occurs in every case (with VIL, VII, and to a lesser extent SHI increasing significantly) with the onset of the first VHF sources. During peak intensity of the cells, the main positive charge region for all but two cells remained above the -20°C isotherm. Although the VHF source density data did show an obvious descent of the upper positive charge region for 13 cases, the descent is much more difficult to discern in the remaining 13 cases.

Five minute running averages of the total flash rates of each cell show the peak flash rates tend to occur at the time of maximum cell intensity as inferred from radar microphysical information. This is likely due to the increase in charge that accompanies an increase in ice available for non-inductive charging. Fig. 3a shows a scatter plot of VII vs. total flash rate for cases associated with the TAMU and Dallas LDAR-II networks, which shows a strong correlation supporting the non-inductive charging hypothesis. Fig. 3b shows a weaker correlation for CG vs. VII, which could be attributed to the complexities involved with CG flashes (e.g. the development of a lower positive region).

As noted by Krehbiel (1996), an increase in updraft strength is responsible for lofting the positive charge region to a higher elevation. Therefore, one would expect an increase in the height of flash origins given a stronger updraft as inferred from radar microphysical information. The 95th percentiles of flash origin heights were plotted against VII for 9 out of the 17 TAMU LDAR-II cases and all nine DFW LDAR-II cases. Figs. 4a and 4b show only a weak correlation between the 95th percentile of flash origin heights and VII for both locations; however, inclusion of all 17 TAMU LDAR-II cases is desired before conclusions are made.

4. DISCUSSION AND CONCLUSIONS

Using 3-dimensional total lightning data, we have provided further evidence supporting the relationship between the convective state of thunderstorms and lightning type and location. The results from 22 out of the 26 cases follow results from several previous studies which show IC lightning dominating in the early stages of vertical development (Williams et al. 1989; Carey and Rutledge 1996). During the initial stages of development, the 30 dBZ contour remained well below the -10°C isotherm in all but one case, suggesting an insufficient quantity of graupel or hail available for the non-inductive charging mechanism (Vincent and Carey, 2004). Not surprisingly, this time did not experience any lightning activity and it was not until the 30 dBZ core began to rise during the onset of rapid intensification that the first lightning flashes tend to occur. This result is similar to previous studies, which suggest that rapid electrical development is associated with the development of mixed-phase precipitation (i.e. graupel and ice crystals in the presence of supercooled water droplets) leading to non-inductive charging as shown by the intensification of the radar echo (e.g., Reynolds and Brook 1956; Krehbiel 1986; Williams 1989; Carey and Rutledge 1996).

For cell 1, the VHF source data suggest the main positive charge region was first approximately along the -18°C isotherm at a height of 7.6 km. As in Krehbiel (1986), this inferred charge region increased to the -30°C isotherm after the cell intensified, resulting in a significant increase in the total flash rate. The main positive charge region remained above the -20°C isotherm during the peak intensity for all but two of the twenty six cells. The increased total flash rates during this time are likely due to the combined effects from the elevated dipole hypothesis (MacGorman et al. 1989) and the increased charge separation occurring in the strong updraft of the cell at this time. In addition, the increase in VII typically corresponded to increased total flash rates (Fig. 3a), suggesting a sufficient amount of ice was available to induce the non-inductive charging mechanism. As the cell starts to weaken, ice particles likely descend resulting in the subsequent formation of a lower positive charge region as inferred by the increase in the percentage of low-level flash origins in cell 1 (e.g., Williams 1989; Williams et al. 1989; Carey and Rutledge 1996).

Comparisons between composite results from both LDAR-II networks in different

meteorological regimes suggest that correlations exist between radar inferred microphysical information and lightning characteristics at each location (Fig. 3a). However, the best fit lines in Fig. 3a show that the nature of the relationship between total lightning and cell intensity differed between the two locations. Further scrutiny of data will determine whether these differences originated from meteorological, instrumentation, and/or algorithmic factors.

Observations from all cases combined indicate that the increases in radar derived intensity parameters correspond to increases in the total flash rate. This suggests that radar parameters can serve as an indication of the total lightning threat. Additionally, total lightning can serve as an indicator of cell intensity with total lightning, over CG, being the preferred choice for accurate inferences on cell intensity.

The analysis of flash origin heights suggests that the data set is not a reliable source of proxy data for cell intensity. However, time periods of low flash rates within each storm appear to be contributing to excess noise within this particular data set. Therefore, further analysis will be made to filter out time periods of low flash rates, which could lead to more robust correlations between flash origin heights and radar inferred microphysical information. In addition, observations of the 90th, 75th, or 50th percentile heights may serve as an additional set of data that could yield less noise than the currently selected 95th percentile. Incorporating slight variations in the time lag between the two data sets could also lead to improvements in the correlations.

Although the results are still in the preliminary stages, these results show that the electrical development and flash characteristics of air mass thunderstorms follow those of more complex modes of convection. Ultimately, this research will lead to important implications for short-term operational forecasting along with an advancement of our basic understanding of cloud electrification. In addition, future research incorporating dual-Doppler analysis from the Shared Mobile Atmospheric Research and Teaching Radar (SMART-R) and the KHGX WSR-88D could provide further insight into the microphysical and kinematical properties associated with total lightning activity.

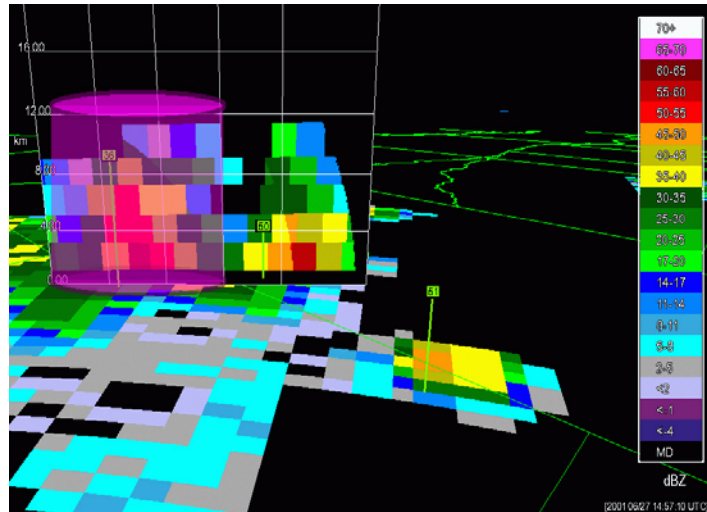
5. REFERENCES

- Byers, H. R., and R. R. Braham Jr., 1949: *The Thunderstorm*. U.S. Govt. Printing Office, 287 pp.
- Carey, L. D., M. J. Murphy, T. L. McCormick, and N. W. S. Demetriades, 2005: Lightning location relative to storm structure in a leading-line trailing-stratiform mesoscale convective system, *J. Geophys. Res.*, **110**, doi:10.1029/2003JD004371.
- Carey, L. D. and S. A. Rutledge, 1996: A multiparameter radar case study of the microphysical and kinematic evolution of a lightning producing storm. *Metr. Atmo. Phys.*, **59**, 33-64.
- Coleman, L. M., T. C. Marshall, M. Stolzenburg, T. Hamilin, P.R. Krshbiel, W. Rison, and R. J. Thomas, 2003: Effects of charge and electrostatic potential of lightning propagation, *J. Geophys. Res.*, **108**(D9), 4298, doi: 10.1029/2002JD002718
- Cummins, K. L., M. J. Murphy, E. A. Bardo, W. L. Hiscox, R. B. Pyle, and A. E. Pifer, 1998: A combined TOA/MDF technology upgrade of the U. S. National Lightning Detection Network. *J. Geophys. Res.*, **103**, 9035-9044.
- Dye, J. E., J. J. Jones, W. P. Winn, T. A. Cerni, B. Gardiner, D. Lamb, R. L. Pitter, J. Hallett, and C. P. R. Sunders, 1986: Early electrification and precipitation development in a small, isolated Montana cumulonimbus. *J. Geophys. Res.*, **91**, 1231 – 1247.
- Ely, B. L., R. E. Orville, and L. D. Carey, 2006: Houston LDAR network performance, data usage, and first results. *Amer. Meteorol. Soc., Second Conference on the Meteorological Applications of Lightning Data*, Paper P2.3
- Hondl, K. D., 2003: Capabilities and components of the Warning Decision Support System – Integrated Information (WDSS-II). Preprints, *19th Conf. On Interactive Info. Processing Systems*, Long Beach, CA, Amer. Meteor. Soc., CD preprints.
- Johnson, J. T., P.L. MacKeen, A. Witt, E. D. Mitchell, G. J. Stumpf, M. D. Eilts, and K. W. Thomas, 1998: The storm cell identification

- and tracking algorithm: An enhanced WSR-88D algorithm. *Wea. Forecasting*, **13**, 263-276.
- Krehbiel, P. R., 1986: The electrical structure of thunderstorms, in *The Earth's Electrical Environment, Studies in Geophysics*, pp. 90-113, National Acad. Sci. Press, Washington, D. C.
- Lang, T. J., and co-authors, 2004a: The Severe Thunderstorm Electrification and Precipitation Study (STEPS). *Bull. Amer. Meteorol. Soc.*, **85**, 1107-1125.
- Lang, T. J., S. A. Rutledge, K. C. Wiens, 2004b: Origins of Positive Cloud-to-Ground Lightning Flashes in the Stratiform Region of a Mesoscale Convective System. *Geophysical Research Letters*, **31**, L10105, 10.1029/2004GL019823.
- Leob, L.B., 1966: The mechanisms of stepped and dart leader in cloud-to-ground lightning strokes. *J. Geophys. Res.*, **71**, 4711-4721
- MacGorman, D. R., and W. D. Rust, 1998: *The Electrical Nature of Storms*, Oxford Univ. Press, New York.
- MacGorman, D. R., D. W. Burgess, V. Mazur, W. D. Rust, W. L. Taylor, and B. C. Johnson, 1989: Lightning rates relative to tornadic storm evolution on 22 May 1981. *J. Atmos. Sci.*, **46**, 221-250.
- Mazur, V., E. Williams, R. Boldi, L. Maier, and D.E. Proctor (1997), Initial comparison of lightning mapping with operational time of arrival and interferometric systems, *J. Geophys. Res.*, **102**, 11,071-11,085.
- Orville, R. E., and G. R. Huffines, 1999: Lightning ground measurements over the contiguous United States: 1995-1997, *Mon. Wea. Rev.*, **127**, 2693-2703.
- Oye, D. and M. Case, 1995: REORDER: A program for gridding radar data. *Installation and use manual for the UNIX version*, NCAR Atmospheric Technology Division, Boulder CO, 19pp.
- Proctor, D. E., 1991: Regions where lightning flashes begin. *J. Geophys. Res.*, **96**, 5099-5112.
- Proctor, D. E., R. Uytendogaardt, and B.M. Meredith, VHF pictures of lightning flashes to ground, *J. Geophys. Res.*, **93**, 12,683-12,727, 1988.
- Reynolds S. E. and M. Brook, 1956: Correlation of the initial electric field and the radar echo in thunderstorms. *J. Atmos. Sci.*, **13**, 376-380.
- Rison, W., R. J. Thomas, P. R. Krehbiel, T. Hamlin, and J. Harlin, 1999: A GPS-based three-dimensional lightning mapping system: Initial observations in central New Mexico, *Geophys. Res. Lett.*, **26**, 1478 – 1489.
- Shao, X. M., and P. R. Krehbiel, 1996: The spatial and temporal development of intracloud lightning, *J. Geophys. Res.*, **101**, 26,641-26,668.
- Steiger, S. M., R. E. Orville, M. J. Murphy, and N. W. S. Demetriades, 2005: Total lightning and radar characteristics of supercells: Insights on electrification and severe weather forecasting. *Amer. Meteorol. Soc., Conference on the Meteorological Applications of Lightning Data*, Paper P1.7.
- Stolzenburg, M., W. D. Rust, and T. C. Marshall, 1998: Electrical structure in thunderstorm convective regions. Part III Synthesis, *J. Geophys. Res.*, **103**, 14097-14108.
- Takahashi, T., 1978: Riming electrification as a charge generation mechanism in thunderstorms. *J Atmos. Sci.*, **35**, 1536-1548.
- Thomas, R. J., P. R. Krehbiel, W. Rison, T. Hamlin, J. Harlin, and D. Shown, 2001: Observations of VHF source powers radiated by lightning, *Geophys. Res. Lett.*, **28**, 143-146.
- Wacker, R. S., and R. E. Orville, 1999a: Changes in measures lightning flash count and return stroke peak current after the 1994 U.S. National Lightning Detection Network Upgrade: 1. Observations, *J. Geophys. Res.*, **104**, 2151-2158.
- Wacker, R. S., and R. E. Orville, 1999b: Changes in measures lightning flash count and return stroke peak current after the 1994 U.S. National Lightning Detection Network Upgrade: 2. Theory, *J. Geophys. Res.*, **104**, 2159-2162.

- Wiens, K. C., S. A. Rutledge, and S. A. Tessendorf, 2005: The 29 June 2000 Supercell Observed During STEPS. Part II: Lightning and Charge Structure. *J. Atmos. Sci.*, **in press**.
- Williams E. R., 1989: The Tripole structure of thunderstorms., *J. Geophys. Res.*, **94**, 13,151 – 13,167.
- Williams E. R., M. E. Webber, R. E. Orville, 1989: The relationship between lightning type and convective state of thunderclouds., *J Geophys. Res.*, **94**, 13,213-13,220.
- Witt, A., M. D. Eilts, G. J. Stumpf, J. T. Johnson, E. D. Mitchell, and K. W. Thomas, 1998: An enhanced hail detection algorithm for the WSR-88D. *Wea. Forecasting*, **13**, 513–518.
- Vincent, B. R. and L. D. Carey, 2004: Using WSR-88D reflectivity data for the prediction of cloud-to-ground lightning: A central North Carolina study., *Natl. Wea. Digst.*, 35-43.

a.



b.

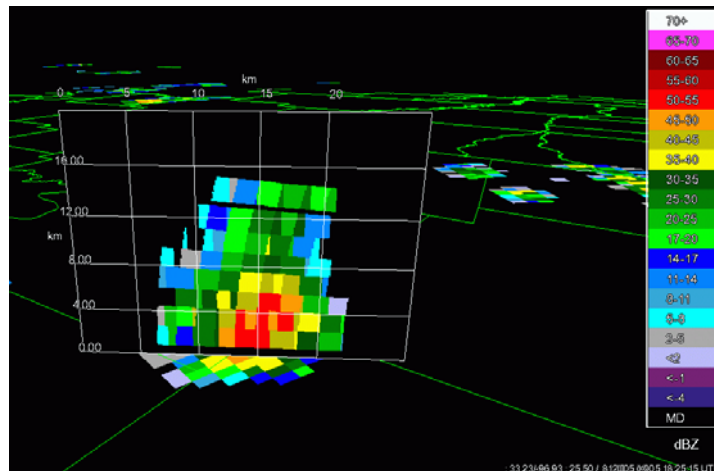
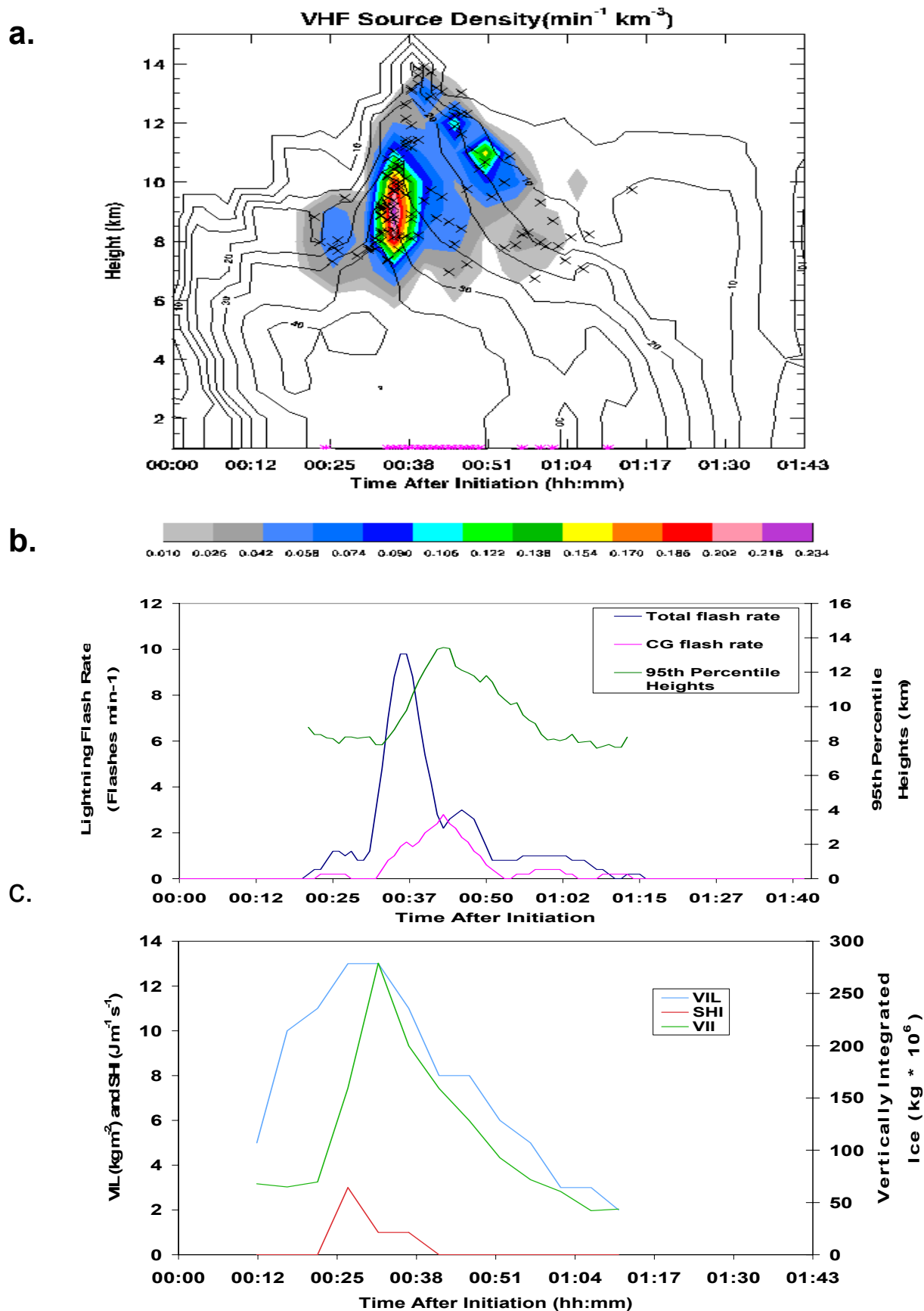


Figure 1. 3-D depiction of radar reflectivity, dBZ shown. a) Vertical cross section taken through a cell occurring on 27 June 2001 during peak intensity at 1457 UTC ($t = 35$ minutes). Shaded cylinder constructed around cell shows bounds of the cell. Cross-section grid box spacing is 4km in the vertical plane and 5km in the horizontal plane. b) Same as (a), but for cell 1 with vertical cross section taken during peak intensity at 1825 UTC ($t = 40$



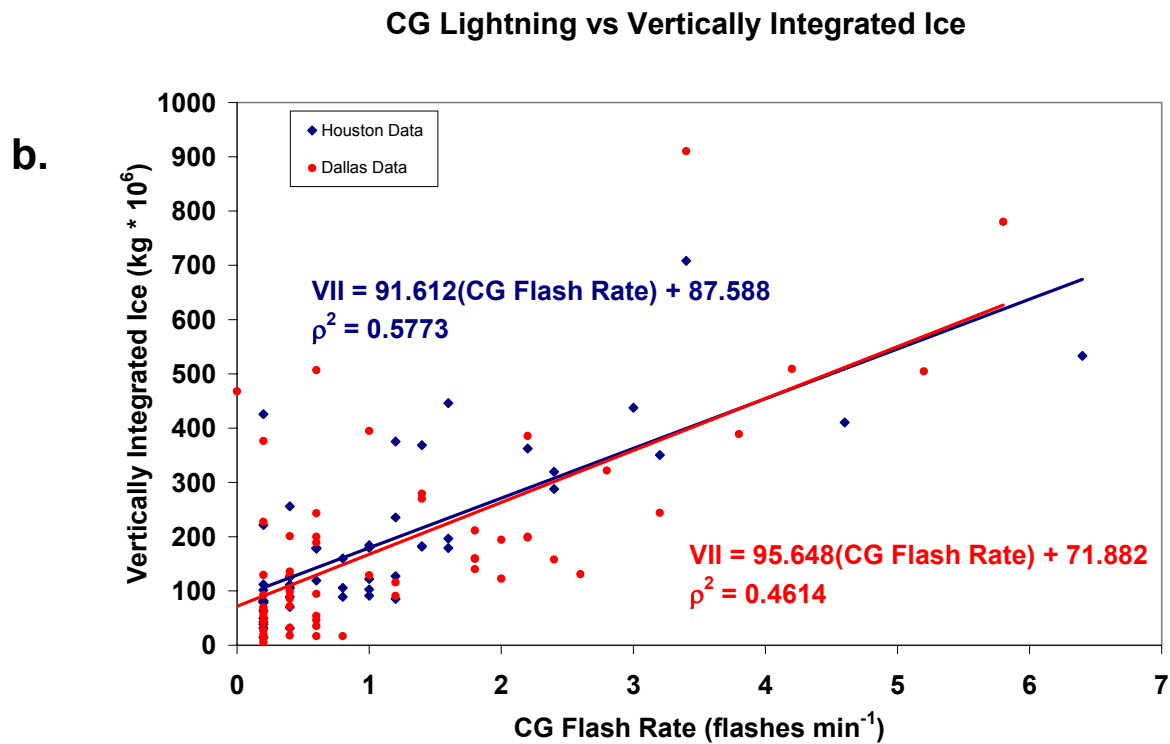
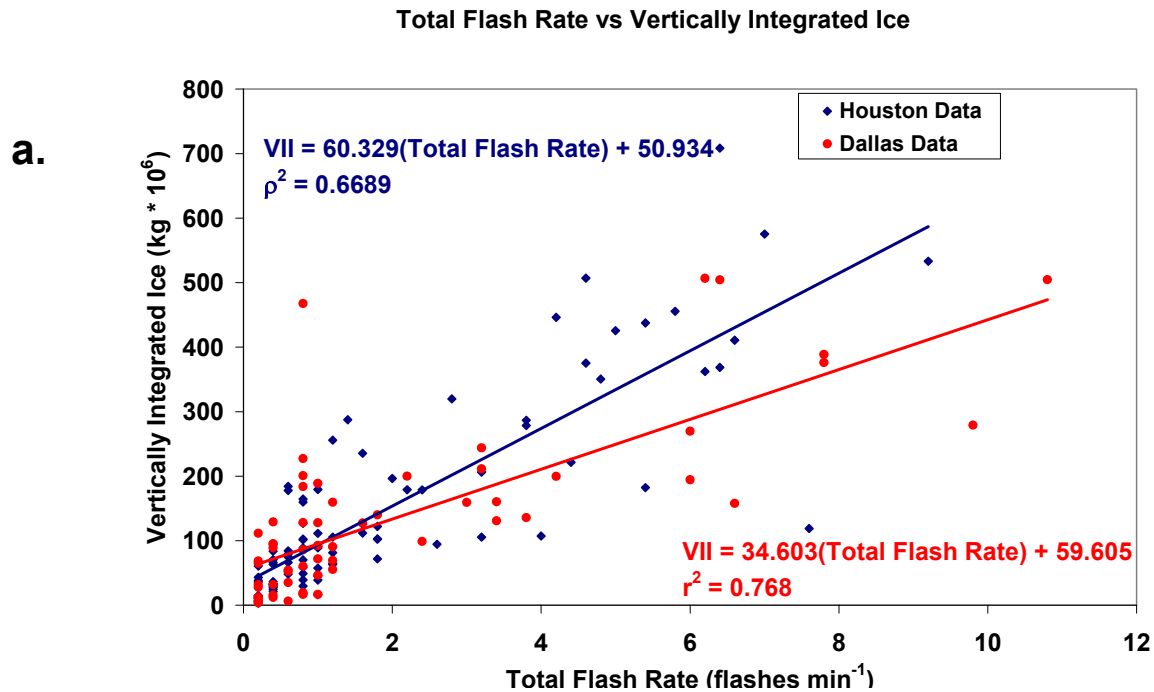
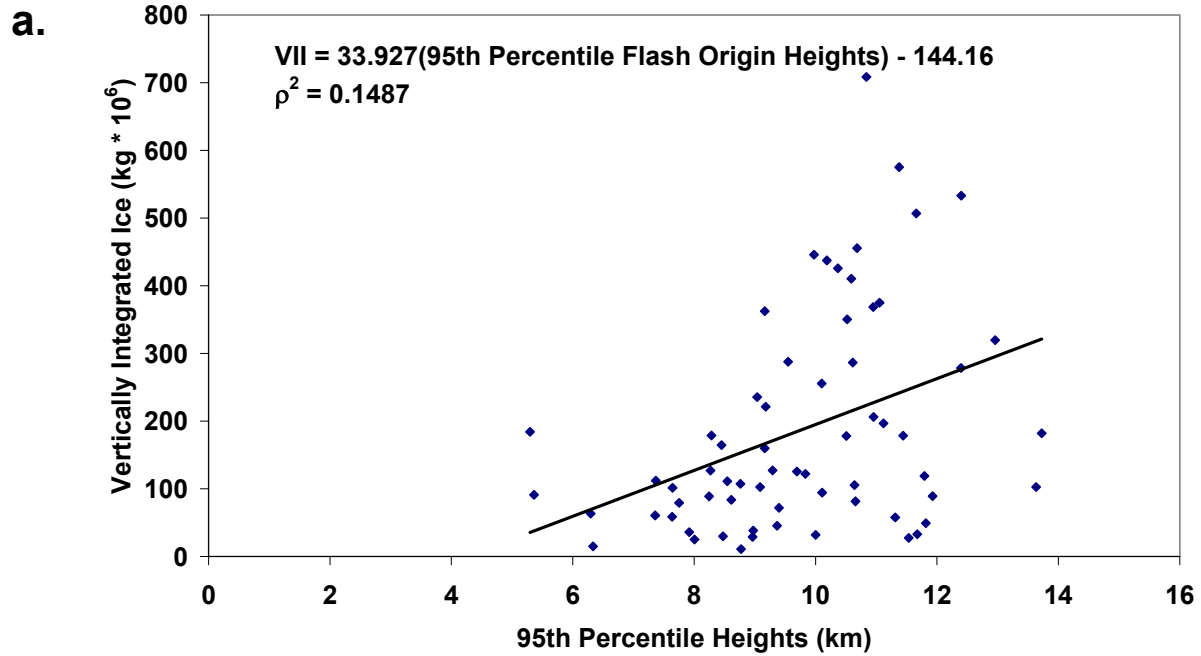


Figure 3. a) Scatter plot of the total flash rate (flashes min^{-1}) vs. vertically integrated ice mass (kg) multiplied by cell area and 10^{-6} for both Dallas and Houston cases. Red points indicate individual data values for Dallas and blue points indicate individual data values for Houston. The red and blue lines represent the equation of best fit for Dallas and Houston data, respectively. The R squared values are also displayed for both Dallas (red) and Houston (blue) showing strong correlations between the total flash rate and vertically integrated ice mass. This strong correlation is likely attributed to increase in charge that occurs with an increase in the ice available for non-inductive charging. b) Same as (a), but with CG flash rate for both Dallas (red points) and Houston (blue points).

95th Percentile Flash Origin Heights vs VII - Houston



95th Percentile Heights vs VII - Dallas

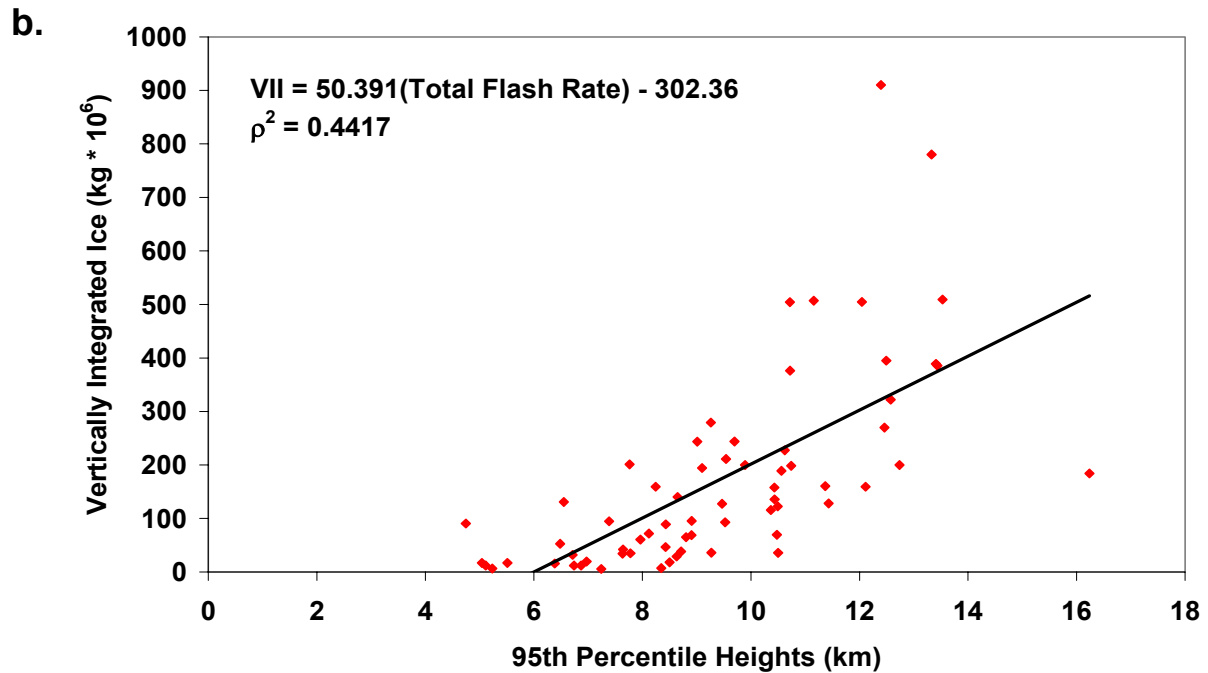


Figure 4. a) Scatter plot of 95th percentile flash origin heights (km) vs. vertically integrated ice mass (kg) multiplied by cell area and 10^{-6} for Houston. Points indicate individual data values, the line represents the equation of best fit. The R squared value is also displayed showing a weak correlation between the 95th percentile flash origin heights and vertically integrated ice mass. b) Same as (a), but with Dallas cases.